Geometry and dynamics of deterministic sand piles

S. H. Liu and Theodore Kaplan
Solid State Division, Oak Ridge National Laboratory, Oak Ridge, Tennessee 37831

L. J. Gray
Engineering Physics and Mathematics Division, Oak Ridge National Laboratory, Oak Ridge, Tennessee 37831
(Received 14 May 1990)

We report a study of the relaxation process of Bak-Tang-Wiesenfeld's sand pile under uniform initial conditions. For most geometries and initial conditions the final states consist of intricate geometric patterns, some of which are self-similar. Even without randomness, the flow of sand during relaxation often displays $1/f$ behavior, and this arises from interactions between the diffusive flow and the development of the final pattern.

I. INTRODUCTION

A wide variety of natural objects are fractals, which means that they look the same under different length scales. Some examples are coastlines, cloud formations, mountain ranges, and distribution of galaxies in the universe.[1] In an analogous situation, many dynamical systems exhibit scale invariance in the time domain. For example, the occurrence of earthquarks follows a seemingly random time sequence, but the sequence looks statistically similar under different time scales. The frequency spectrum of such a sequence rises in the low-frequency end. Other examples of this so-called $1/f$ fluctuation are found in sun-spot activities, traffic flow, the flow of sand in an hour glass, and the flow of electric current through a resistor.[2]

The close analogy between spatial and temporal scale invariance leads one to ask whether the two phenomena may evolve from a common origin. A link between the two was proposed recently by Bak, Tang, and Wiesenfeld[3-5] (BTW) in terms of a concept called "self-organized criticality." They argued that dynamical systems with extended degrees of freedom naturally develop into a critical state without detailed specification of the initial conditions. Perturbations of these critical states result in changes in the system which show both spatial and temporal scaling, suggesting that there is an intimate connection between the two phenomena. As a concrete example, BTW studied a cellular automaton model for sand in a box. The model is based on the observation that a pile of sand will collapse once its slope exceeds a critical value. A critical state may be created in two ways, by dropping sand randomly in an empty box and letting the pile relax whenever the local slope exceeds the critical value, or by relaxing a random pile for which the local slope at every point is above critical.

In this paper we report a series of studies of the relaxation process of the same model under deterministic conditions, namely uniform, but above critical initial slopes. Despite the lack of randomness, the relaxation process exhibits $1/f$ behavior under a variety of circumstances. The fully relaxed states often have complex distributions of slopes, and some of the patterns are self-similar. The temporal scaling is intimately linked to the growth of the spatial pattern. This demonstrates for the first time that $1/f$ fluctuations can be the result of diffusion through self-generated complex patterns.

II. SAND-PILE MODEL

To define the model we erect a regular lattice in a D-dimensional space and associate a scale $Z(\mathbf{R}_l)$ with every lattice point $\mathbf{R}_l$. If m denotes the number of nearest neighbors of every lattice point, then the following rules define the dynamics of the model: (i) if $Z(\mathbf{R}_l)<m$, the point $\mathbf{R}_l$ is said to be stable and $Z(\mathbf{R}_l)$ remains unchanged; and (ii) if $Z(\mathbf{R}_l)>m$, we redistribute Z according to

$$\begin{aligned} &Z(\mathbf{R}_l)\rightarrow Z(\mathbf{R}_l)-m\ , \\ &Z(\mathbf{R}_l+\boldsymbol{\delta}_i)\rightarrow Z(\mathbf{R}_l+\boldsymbol{\delta}_i)+1\ , \end{aligned} \tag{1}$$

where $\boldsymbol{\delta}_i$ for $i=1,2,\ldots,m$ denote the set of vectors linking a lattice point to its nearest neighbors. In the event that many sites have $Z>m$, all are relaxed simultaneously. This is a cellular automaton for which the discrete variables $Z(\mathbf{R}_l)$ at time $t+1$ depend on the Z's at $\mathbf{R}_l$ and all of its neighbors at time t. The variable Z is not conserved at boundary sites, as one unit of Z can be lost for every nearest-neighbor site outside the boundary. This is defined as the "closed boundary" by BTW.[5,6]

The physical meaning of the model is obvious when one considers the one-dimensional (1D) case. The variable Z is the local slope of a discretized sand pile, and $m=2$ is the critical slope. When extended to higher dimensions, the meaning of Z is less tangible. Strictly speaking the local slope for two- or three-dimensional sand piles is a vector quantity, but is represented by a scalar in the model. On the other hand, if one regards Z as a local charge distribution, the model may be a reasonable simulation of the flow of charges in a fast-ion conductor.[7] Similarly, it may also be a crude model of the flow of fluxoids in type-II superconductors above the flux lattice melting temperature.[8] For these reasons, the

 ©1990 The American Physical Society

model is of interest in condensed-matter physics. In the subsequent discussion we will continue to refer to Z as the "slope."

If one starts with a distribution of slope such that every lattice points has $Z \gg m$, the rules of redistribution map exactly onto the diffusion equation. Because Z is dissipated by flowing out of the boundary, the slopes at some points eventually reach m or below and the diffusion through those sites is temporarily halted. This introduces nonlinearity into the system and gives rise to numerous interesting geometric and dynamic properties. The self-organized critical cluster in the original work of BTW was constructed by starting with a random distribution of Z, all greater than m, and applying the rules in Eq. (1) until every point became stable. The resulting clusters appear random, but when disturbed, the time it takes for the perturbation to spread out is linked to the size of the region in which the disturbance is felt. In this manner a relation is established between spatial and temporal scaling.

In our studies we start with uniform initial distributions of $Z = Z_0 > m$ at every lattice point and investigate the geometric properties of the final distribution and the dynamics of the relaxation process. While it is intuitively obvious that the flow of slope out of the boundary will eventually cause the process to stop, it is difficult to make this idea precise. The following simple argument provides a proof that the relaxation terminates in a finite time. We define the second moment of the distribution of Z by

$$M = \sum_l Z(\mathbf{R}_l)|\mathbf{R}_l|^2 , \tag{2}$$

and calculate the change of M after every iteration. It is easy to show that for every interior point with $Z > m$, the redistribution increases the second moment by m. The same result holds also for boundary points provided that we add another layer of points just outside the boundary to collect all Z's lost at the boundary. The value of M increases at every iteration as long as there is at least one unstable point and regardless of whether some Z's is lost at the boundary or not. On the other hand, M cannot increase without limit because it has an absolute upper bound, i.e., the impossible situation where all Z's are moved outside the boundary and collected at the corners. Therefore the process must stop when M ceases to increase, corresponding to the state in which all Z's are equal to or less than m. The properties of the final state will be discussed in Sec. III.

III. GEOMETRY OF RELAXED STATES

The relaxed state is the final distribution of slopes when the redistribution process stops. The slope at every lattice point is less than or equal to m. Consider a square grid with $m=4$. Starting with an initial distribution $Z_0=5$, we obtain the final cluster shown in Fig. 1. The pattern in each quadrant consists of a set of nesting heart shapes along the diagonal with nonuniform slope inside and surrounded by regions of uniform slope $Z=4$. The ratios of the linear measures of the nearest pair of heart shapes are rational approximations of the irrational quantity $a=(3-\sqrt{5})/2$, which is the classic Golden Section ratio. We deduced this result by using a combination of geometric and empirical reasoning. An outline of the pattern in one quadrant in shown in Fig. 2. The vertices on the boundary are denoted by A_1, A_2, A_3, etc., those on the diagonal by O, O_1, O_2, etc., and the projections of points O onto the boundary by B_0, B_1, B_2, etc. We find empirically that every A point divides the segment between the pair of B points on either side in approximately a constant ratio, and every B point divides the segment between the pair of A points on either side in the same ratio. This allows us to write for the ideal case of an

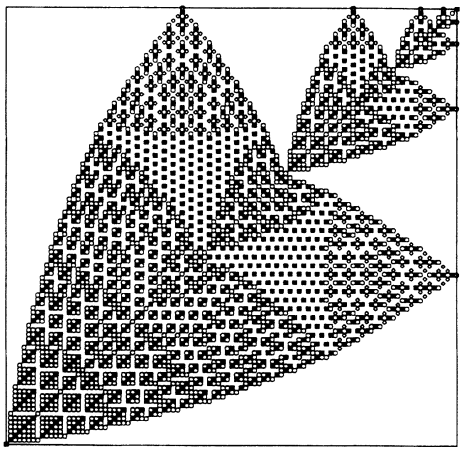

FIG. 1. Final slope distribution for a square sand pile with square grid ($m=4$) under the initial condition $Z_0=5$. Only one quadrant is shown, with the center of the square at the lower left corner. The values of Z at various points are coded as follows: 1 by squares, 2 by diamonds, 3 by open circles, and 4 by open space.

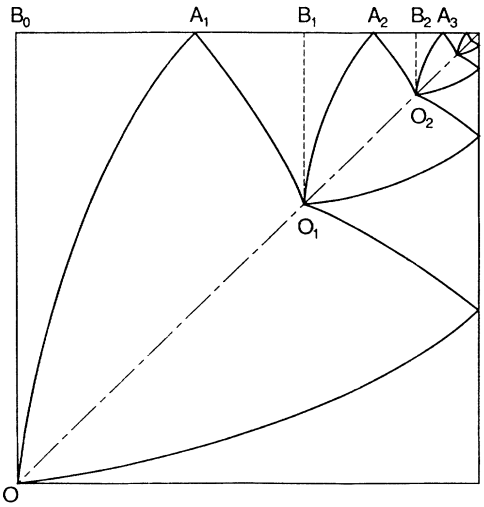

FIG. 2. Outline of the pattern in Fig. 1.

infinite system that

$$A_1B_1/B_0A_1 = B_1A_2/A_1B_1 = A_2B_2/B_1A_2 = \cdots = r \ . \tag{3}$$

We also find that $B_0A_1 = A_1A_2$ to within one lattice point for systems of various sizes. Therefore, for an infinite system we have $1 = r + r^2$. The solution of this equation is $r = (\sqrt{5}-1)/2$, and the scaling ratio is $a = r^2 = (3-\sqrt{5})/2$.

The boundaries of the heart shape around the vertex on the diagonal are described by the fractional power parabolas $x = Ay^{\alpha}$ and $y = Ax^{\alpha}$. The exponent α is determined empirically to be approximately 1.2. The boundaries around the other vertices are also given by these parabolas after suitable rotations of axes.

For larger values of initial slope Z_0 the final patterns are more complex, but remain self-similar. The final pattern for $Z_0 = 6$ is shown in Fig. 3. In general, we obtain $Z_0 - 4$ branches of nesting heart shapes in each quadrant. Spatial scaling is obeyed near the corners. With more branches the heart shapes are smaller and the scaling ratios are closer to unity. We noticed that for $Z_0 = 5$ the vertex of the second largest heart shape at the boundary coincides within one lattice point with the vertex of the third largest shape for $Z_0 = 6$, and with that of the fourth largest shape for $Z_0 = 7$, etc. An argument similar to that in the $Z_0 = 5$ case allows us to establish the scaling ratio for general Z_0 as $a^{3/(2Z_0-7)}$. The boundaries between uniform and nonuniform regions are described by the same fractional power parabolas. We have also studied a cubic system ($m = 6$) with initial conditions $Z_0 = 7$, 8, and 9. The cross section of the 3D patterns with the [100] plane are 2D patterns very similar to those of the square system. The scaling ratios are given by powers of a and the boundaries of the nonuniform regions are described by the same parabolas. The fact that a and α are not sensitive to the spatial dimension implies that they are not critical exponents.

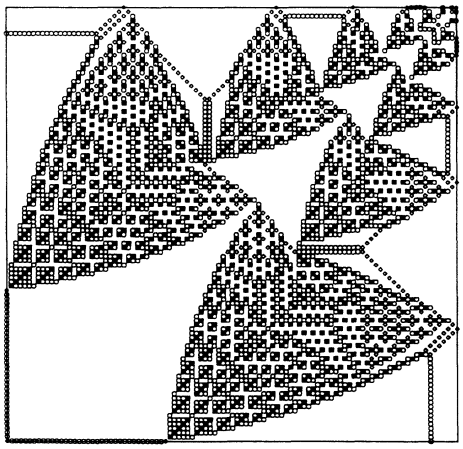

FIG. 3. First quadrant of the final pattern for a square sand pile with square grid under the initial condition $Z_0 = 6$. The Z values are coded as in Fig. 1.

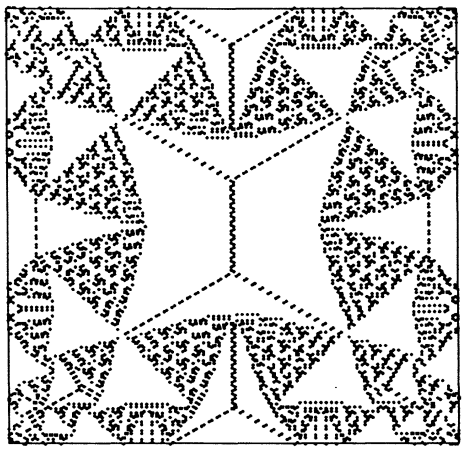

FIG. 4. Final slope distribution for a square sand pile with honeycomb grid ($m = 3$) under the initial condition $Z_0 = 4$. The code is 1 represented by squares, 2 by diamonds, and 3 by open space.

To study the dependence of the geometry on the grid, we enclose honeycomb ($m = 3$) and triangular ($m = 6$) grids in square boundaries. The final states have different patterns, but the scaling ratios and the exponent α are the same as for the square grid. The pattern for the honeycomb grid with $Z_0 = 4$ is shown in Fig. 4.

In Fig. 5 we show a final pattern that is nonfractal. This is obtained by enclosing a honeycomb grid in an equilateral triangle with starting slope $Z_0 = 4$. This pattern maps onto the solution of fitting three largest regular nanogons within the triangle in that the vertices of the nanogons on the border coincide within one mesh point with the corners of the round shapes. It also maps onto a tiling problem involving regular triangles, nanogons, and three-pointed six-sided stars. The stars have vertex angles equal to 20°. The outlines of the three kinds of tiles are shown in Fig. 6. Within each round shape one can

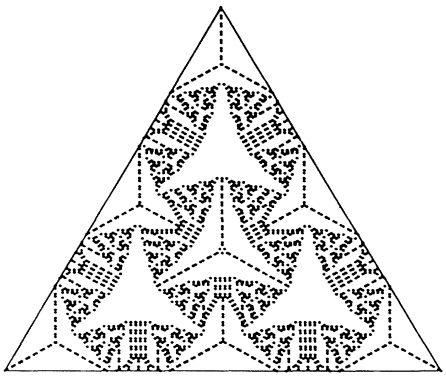

FIG. 5. Final pattern for a triangular sand pile with honeycomb grid under the initial condition $Z_0 = 4$. The code is 1 represented by squares, 2 by diamonds, and 3 by open space. It is difficult to distinguish between 1 and 2 because of the finess of the grid, but 1 occurs very infrequently.

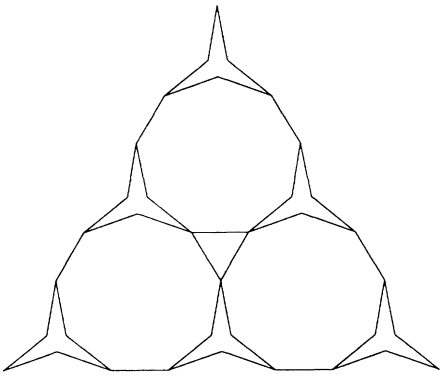

FIG. 6. Tiling pattern that is isomorphic to the pattern in Fig. 5.

discern three regions bounded by the 1.2 power parabolas. For higher values of Z_0 the patterns map onto the same tiling problem with $(Z_0-1)(Z_0-2)/2$ nanogons within the border. For a triangular grid inside the same equilateral triangular boundary the patterns depend on whether Z_0 is odd or even. Odd values of Z_0 produce patterns isomorphic to those obtained on the honeycomb lattice, whereas even values of Z_0 produce simple checkerboard patterns with triangular regions of uniform $Z=4$ and 6.

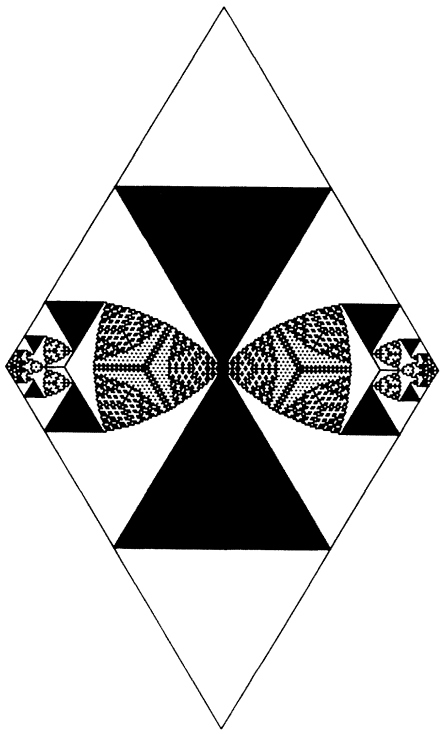

FIG. 7. Final slope distribution for a diamond shaped sand pile with triangular lattice ($m=6$) under the initial condition $Z_0=8$. The grid is too fine to allow clear resolution of Z values in the final state, so we coded all points with $Z<6$ by black dots and $Z=6$ by open space. This gives a clear picture of the nonuniform part of the final pattern.

Regions bounded by obtuse angles give rise to complex patterns that cannot be described by a constant scaling ratio. As an example, we show in Fig. 7 the final pattern obtained for a triangular grid in a diamond shaped boundary with $Z_0=8$. The equilateral triangles of various sizes are all regions of uniform $Z=4$. The pattern appears increasingly more complex as one approaches the 120° corners, and this is a clear indication of the breakdown of uniform scaling. From a large number of patterns we have gathered so far, we find uniform scaling only in regions bounded by right angles.

IV. DYNAMIC PROPERTIES

As was pointed out earlier, the laws of redistribution in Eq. (1) map exactly onto the diffusion equation when the slopes at all points are much higher than the critical slope m. If one starts with $Z_0>m$, one should find the classical behavior in the flow of Z during the early stages of the relaxation process. We have studied this by counting the total Z collected outside the boundary as a function of time t, which is the number of iterations. Independent of Z_0, the grid and the boundary, we obtain the total flow to be proportional to $t^{1/2}$ at small t as expected. Later in the process the flow slows down and in the square system the total flow takes on a different power-law dependence with the exponents 0.40, as shown in Fig. 8. This behavior is known as anomalous diffusion, and we will show in the following that anomalous diffusive systems also have the $1/f$ noise spectrum.

In classical diffusion the total charge $Q(t)$ is proportional to $t^{1/2}$. If in a critical system time scales according to the dynamical scaling exponent $t^{1/z}$,[9] then we expect $Q(t)\sim t^{1/2z}$ for diffusion in such a system. When a classical system is driven by a constant external potential, the

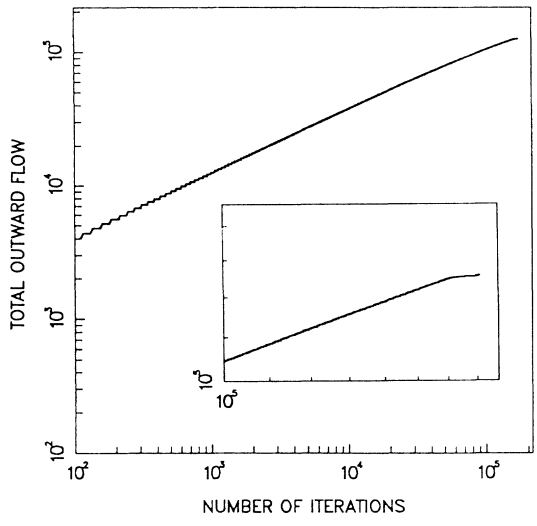

FIG. 8. Total outward flow of Z for a 801×801 square sand pile as a function of time t, which is measured by the number of iterations. During the first 1000 steps the total flow follows the $t^{1/2}$ law, indicating classical diffusion. The insert shows the flow curve during the last 70 000 of the more than 170 000 steps, illustrating the $t^{0.4}$ law of anomalous diffusion.

current follows the Ohm's law and the total charge $Q(t)$ is proportional to t. In an analogous situation, a driven anomalous diffusive system gives $Q(t) \sim t^{1/z}$. The current is given by $I(t) \sim t^{-(1-1/z)}$, and its frequency spectrum given by $I(\omega) \sim \omega^{-1/z}$. The power spectrum is proportional to $|I(\omega)|^2$, and thus has the frequency dependence $\omega^{-2/z}$. From the result in Fig. 8, we can determine the frequency exponents $2/z = 1.6$ for the square system. We have also studied the cubic system and obtained $2/z = 1.0 \pm .04$. Bak, Tang, and Wiesenfeld determined the frequency exponents by perturbing the self-organized critical clusters, and they reported the values 1.57 and 1.08 for 2D and 3D systems, respectively.[1] There is good agreement between these two different ways of calculating the frequency exponents.

Examination of the intermediate patterns during the relaxation process reveals an intimate connection between anomalous diffusion and the growth of the complex pattern in the final state. In Fig. 9 we show four intermediate patterns for the square system with $Z_0 = 5$. Very early in the relaxation process the uniform distribution breaks down into plane waves with crests of $Z = 6$ and troughs of $Z = 4$, as shown in Fig. 9(a). A rudimentary heart shape develops at the corner, and it interacts with the waves and changes the crest and trough values to 5 and 3. A thin strip of uniform $Z = 4$ separates the front of the waves from the boundary. As time progresses the wave front moves toward the boundary, and upon reaching it ejects a pulse of Z. Afterwards the wave front retreats toward the center until it reaches the tip of the heart shape. At this point the motion reverses itself and the shape grows by one grid point. At a later time, shown in Fig. 9(b), the shape has grown in size, and smaller shapes have formed following the wake of the leading one. The growth of the nonuniform region causes the width of the wave front to shrink and the distance traversed by the wave front to lengthen. Consequently, every time the wave front returns to the boundary, it

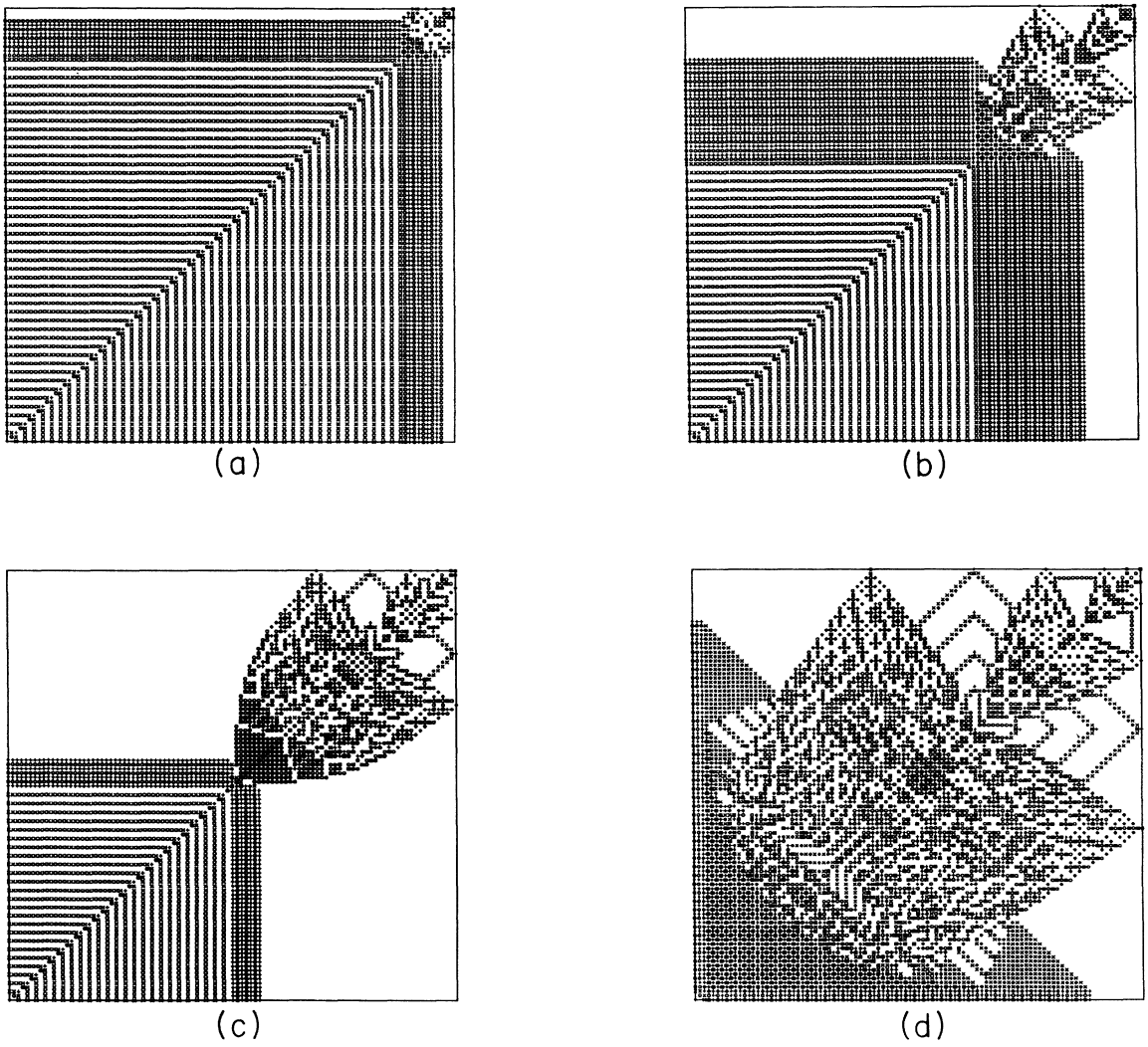

FIG. 9. Four intermediate stages of the development of the final pattern in Fig. 1. In addition to the four codes used in Fig. 1, we need 5 represented by pluses, 6 by crosses, and 7 and 8 by asterisks. The last two values occur infrequently. The number of iterations are (a) 160, (b) 1320, (c) 2608, and (d) 9690. It required 10 738 iterations to reach the final state.

ejects a pulse that is two units less than the previous one, and the interval between successive pulses increases by two units. The total flow after t iterations is given by

$$Q(t)=\sum_n [N-2(n-1)]\delta_{t,n^2-n+1}\simeq Nt^{1/2} \quad (4)$$

for $1 \ll t \ll N$. In Eq. (4) N is the size of the boundary and n sums over the sequence of pulses. The δ function indicates that the nth pulse emerges at $t=n^2-n+1$. We identify this contribution as the classical component of the diffusion process.

As the nonuniform region grows to about one-half of its final size, shown in Fig. 9(c), we can clearly see waves flowing toward the boundary in the region between some of the shapes. The wave fronts make 45° angles with the boundary. The excess Z in these waves must first flow through the leading shape, and are ejected at the boundary sporadically. We identify this as the emerging anomalous diffusion component. Near the end, shown in Fig. 9(d), the classical diffusion component becomes insignificant and the anomalous component dominates the total flow. This sequence of events demonstrates that the anomalous behavior is due to flows through the nonuniform part of the intermediate distribution. The close analogy with the diffusion in random network problem[10] or the ant in the labyrinth problem is quite apparent.[11] The only difference is that the system creates its own labyrinth, and the self-generated structure is a unique feature of the sand-pile model.

During the growth process the nesting heart shapes maintain their scaling ratio. This indicates that the ratio is determined by the angle between the boundary lines and the value of Z_0. The other two boundaries play no role except to determine the size of the final pattern.

For systems whose adjacent boundaries form only acute or obtuse angles, the total flow also tends to slow down but there is no well-defined exponent for anomalous diffusion, and thus no clear indication of temporal scaling. The final patterns of these systems do not show constant spatial scaling, so it appears that constant temporal scaling is associated with the growth of a self-similar pattern.

V. CONCLUSIONS

The states we have studied do not fall into the category of self-organized critical states because they are clearly sensitive to the initial condition as well as the boundary condition. Perturbations on these states do not necessarily generate disturbances that exhibit spatial and temporal scaling. Our findings demonstrate that large systems with nonlinear diffusive properties can spontaneous evolve into complex spatial patterns under completely deterministic initial conditions. Furthermore, the growth of the spatial pattern hinders the diffusive flow in such a way that if the pattern is self-similar in space, the fluctuation in the flow can be self-similar in time. This may shed new light on the physical origin of the ubiquitous $1/f$ noise.

ACKNOWLEDGMENTS

One of the authors (S.H.L.) would like to thank P. Bak for helpful discussions. We are also indebted to Lisabeth Skodvin for preparing a video of the relaxation of a square sand pile and to N. Modine for writing many of the computer programs. This work was supported by the U.S. Department of Energy, Division of Basic Energy Sciences, under Contract No. DE-AC005-84OR21400 with Martin Marietta Energy Systems, and by the IBM Bergen Scientific Centre, Bergen, Norway.

[1]B. B. Mandelbrot, *Fractals: Forms, Chance and Dimension* (Freeman, San Francisco, 1977); *The Fractal Geometry of Nature* (Freeman, San Francisco, 1983).

[2]For a review of $1/f$ noise, see W. H. Press, Commmun. Mod. Phys. C 7, 103 (1978).

[3]P. Bak, C. Tang, and K. Wiesenfeld, Phys. Rev. Lett. **59**, 381 (1987).

[4]C. Tang and P. Bak, Phys. Rev. Lett. **60**, 2347 (1988).

[5]P. Bak, C. Tang, and K. Wiesenfeld, Phys. Rev. A **38**, 364 (1988).

[6]The "closed" boundary conserved sand but not slope. Conversely, the "open" boundary conserved slope but not sand. See Ref. 3 for details.

[7]W. van Gool, in *Solid Electrolytes: General Principles, Characterization, Materials, Applications,* edited by P. Hagenmuller and W. van Gool (Academic, New York, 1978), Chap. 1.

[8]Melting of flux lattice was first reported for the high-T_c superconductors by P. L. Gammel, D. J. Bishop, G. J. Dolan, J. R. Kwo, C. A. Murray, L. F. Schneemeyer, and J. V. Waszczak, Phys. Rev. Lett. **59**, 2592 (1987).

[9]A comprehensive discussion of dynamical scaling can be found in S.-K. Ma, *Modern Theory of Critical Phenomena* (Benjamin, Reading, MA, 1976), Chap. 13.

[10]For a comprehensive review of the diffusion in random network problem see S. H. Liu, in *Solid State Physics,* edited by H. Ehrenreich and D. Turnbull (Academic, Orlando, 1986), pp. 244–257.

[11]P. G. de Gennes, Recherche **7**, 919 (1976).